frontiers in Materials

ORIGINAL RESEARCH
published: 26 January 2022
doi: 10.3389/fmats.2022.839948

# Eco-Friendly Anticorrosion Superhydrophobic $Al_2O_3$@PDMS Coating With Salt Deliquescence Self-Coalescence Behaviors Under High Atmospheric Humidity

*Binbin Zhang[1,2,3]*, Jiayang Yan[1], Weichen Xu[1], Teng Yu[1], Zhuoyuan Chen[4] and Jizhou Duan[1,2,3]*

[1]CAS Key Laboratory of Marine Environmental Corrosion and Bio-fouling, Institute of Oceanology, Chinese Academy of Sciences, Qingdao, China, [2]Open Studio for Marine Corrosion and Protection, Pilot National Laboratory for Marine Science and Technology (Qingdao), Qingdao, China, [3]Center for Ocean Mega-Science, Chinese Academy of Sciences, Qingdao, China, [4]School of Materials Science and Hydrogen Energy, Foshan University, Foshan, China

Bio-inspired superhydrophobic coatings have been demonstrated to be promising anticorrosion materials. However, developing robust superhydrophobic coatings through simple one-step fluorine-free procedures to meet various functional requirements remains a major challenge. In this study, we fabricated an eco-friendly superhydrophobic $Al_2O_3$@PDMS composite coating with mechanical robustness based on $Al_2O_3$ NPs, PDMS, and spray coating technique. To characterize surface morphologies, chemical compositions, surface wettability, and anticorrosion properties, FE-SEM, EDS, XPS, contact angle meter, electrochemical impendence spectroscopy, and potentiodynamic polarization techniques were employed. The electrochemical results show that $|Z|_{0.01\ Hz}$ and $R_{ct}$ values of the superhydrophobic $Al_2O_3$@PDMS coating were four orders of magnitude higher than bare Q235 carbon steel, indicating a significant improvement in corrosion resistance. Furthermore, the deliquescence behaviors of NaCl salt particles and the instantaneous self-coalescence phenomenon were recorded under high atmospheric humidity to suggest that a superhydrophobic surface with Cassie–Baxter interfacial contacts can serve as an efficient barrier to suppress the formation of saline liquid thin films and protect the underlying substrate from corrosion. This robust superhydrophobic $Al_2O_3$@PDMS coating is expected to be easily applied to a variety of substrates and to find potential applications for liquid repellency, self-cleaning, corrosion resistance, and other properties.

**Keywords: anticorrosion, superhydrophobic, fluorine-free, salt deliquescence, atmospheric corrosion**

OPEN ACCESS

***Edited by:***
*Changdong Gu,*
*Zhejiang University, China*

***Reviewed by:***
*Sudagar J.,*
*VIT-AP University, India*
*Liang Wu,*
*Chongqing University, China*

****Correspondence:***
*Binbin Zhang*
*zhangbinbin11@mails.ucas.ac.cn*

***Specialty section:***
*This article was submitted to Environmental Degradation of Materials, a section of the journal Frontiers in Materials*

***Received:*** *20 December 2021*
***Accepted:*** *10 January 2022*
***Published:*** *26 January 2022*

***Citation:***
*Zhang B, Yan J, Xu W, Yu T, Chen Z and Duan J (2022) Eco-Friendly Anticorrosion Superhydrophobic $Al_2O_3$@PDMS Coating With Salt Deliquescence Self-Coalescence Behaviors Under High Atmospheric Humidity. Front. Mater. 9:839948. doi: 10.3389/fmats.2022.839948*

## INTRODUCTION

Carbon steels are widely used for structural applications in industrial and engineering constructions because of their high specific strength, weldability, machinability, and low cost (Oguzie et al., 2010; Zhang S. et al., 2020; Tan et al., 2020). However, the aggressive nature of different service environments causes serious corrosion and degradation of exposed carbon

steels, resulting in massive economic loss and inevitable safety accidents. Extensive studies indicate that the use of multifunctional protective coatings is one of the most effective strategies for reducing the tendency of metallic corrosion (Ye et al., 2020; Panda et al., 2021). In recent years, the development of bio-inspired superhydrophobic coatings has become one of the anticorrosion research hot spots because it can provide a non-wetting physical barrier between the metallic surface and the surrounding environments (Du and Chen, 2020; Zhang ZQ et al., 2020; Jena et al., 2020; Darband et al., 2020; Zhang and Xu, 2021; Zhang ZQ et al., 2021; Zhang B et al., 2021).

Nature-inspired superhydrophobicity refers to the surface with a static water contact angle greater than 150° and a sliding angle less than 10° (Esmaeili et al., 2020). Micro-/nano-/binary rough structures and low surface energy are the two essential parameters for designing superhydrophobic materials. To develop superhydrophobic surfaces, a variety of technologies including chemical etching (Zhang et al., 2019b; Lan et al., 2021), anodization (Mokhtari et al., 2017; Zhang et al., 2019a), hydrothermal (Wang and Guo, 2018; Zhang B et al., 2021), and laser processing (Boinovich et al., 2018; Sataeva et al., 2020) have been introduced. Despite significant advances in scientific community, many limitations remain in large-scale fabrication and widespread practical applications, such as strict experimental conditions, complicated preparation procedures, and fluorine-containing toxic compounds (Anitha et al., 2018; Wang and Zhang, 2020). Given these concerns, it is particularly significant to design and develop facile one-step, low cost, and fluorine-free eco-friendly superhydrophobic coatings for efficient anticorrosion applications.

Thus, in this study, fluorine-free PDMS with intrinsic hydrophobicity and $Al_2O_3$ nanoparticles ($Al_2O_3$ NPs) were employed to design and fabricate the superhydrophobic $Al_2O_3$@PDMS composite coating through a facile one-step spray coating technique. The evolution of surface wettability with different $Al_2O_3$ NPs/PDMS mass ratios was investigated. The dynamic water droplet contacting process, surface morphologies, chemical compositions, anticorrosion properties, NaCl salt deliquescence behaviors, and mechanical stability were systematically studied. The results show that this substrate-independent superhydrophobic $Al_2O_3$@PDMS composite coating exhibits superior adaptability and corrosion suppression performance.

# EXPERIMENTAL SECTION

## Materials and Reagents

Q235 carbon steel substrates (size: 40 mm × 40 mm × 1 mm) were purchased from Shandong Shengxin Technology Co., Ltd. Hydrophilic aluminum oxide nanoparticles ($Al_2O_3$ NPs, 99.9%, 30 nm) were purchased from Shanghai Macklin Biochemical Co., Ltd. Polydimethylsiloxane (PDMS, Sylgard 184) and silicone elastomer curing agent were obtained from Dow Corning Corporation. Other reagents including n-hexane ($C_6H_{14}$, 97.0%), ethanol absolute ($C_2H_6O$, 99.7%), sodium chloride (NaCl, 99.5%), and methylene blue trihydrate ($C_{16}H_{18}ClN_3S{\cdot}3H_2O$, 99.5%) were supplied by Sinopharm Chemical Reagent Co., Ltd, and 3 M VHB tape was supplied by 3 M China Limited. Silicon carbide abrasive paper (2000 grit) was provided by Suisun Co., Ltd. All chemical reagents were used as received without further purification.

## Fabrication of Superhydrophobic $Al_2O_3$@PDMS Coating

A total of 1 g PDMS, 0.1 g curing agent, and different amounts of $Al_2O_3$ NPs were ultrasonically and magnetically dissolved in 10 ml n-hexane to obtain a milk-like suspension. Different mass ratios of $Al_2O_3$ NPs/PDMS (1:4, 1:2, 3:4, 1:1, 5:4, and 3:2) were used to achieve $Al_2O_3$@PDMS composite coatings. Prior to the spray coating process, Q235 carbon steel substrates were sanded and cleaned with ethanol absolute solution. A spraying gun with a nozzle diameter of 1 mm and a spraying pressure of 0.3-MPa was employed for spray coating treatment. The spray-coated $Al_2O_3$ NPs/PDMS composite coatings were cured at 100°C for 1 h after spraying. Various substrates including glass, aluminum alloy, 3D foam material, polyurethane plastic, wood, filter paper, and concrete block were used to prepare superhydrophobic $Al_2O_3$@PDMS coating according to the same procedure of Q235 carbon steel. The schematic illustration of the preparation process of the superhydrophobic $Al_2O_3$@PDMS composite coating is shown in **Figure 1**.

## Characterizations

The micro-/nano-morphologies of different samples were observed by using a field-emission scanning electron microscope (FE-SEM, FEI Nova Nano SEM450) equipped with energy-dispersive X-ray spectroscopy (EDS, Oxford X-MaxN50). X-ray photoelectron spectroscopy (XPS, Thermo Scientific Escalab 250Xi) was employed to analyze the chemical compositions of the fabricated superhydrophobic $Al_2O_3$@PDMS composite coating. The static water contact angles and sliding angles of $Al_2O_3$@PDMS composite coatings with different $Al_2O_3$/PDMS mass ratios were measured by a contact angle meter (Dataphysics OCA25) with 4 μL deionized water droplets.

## Electrochemical Tests

The electrochemical tests of different samples were carried out using an electrochemical workstation (CorrTest CS2350H) in a typical three-electron cell. Platinum sheet, saturated calomel electrode, and testing samples were used as the counter electrode, the reference electrode, and the working electrode, respectively. The electrochemical impendence spectroscopy (EIS) and the potentiodynamic polarization of bare Q235 carbon steel and superhydrophobic $Al_2O_3$@PDMS composite coating were measured in 3.5 wt.% NaCl aqueous solution under open circuit potential with an amplitude of 10 mV. The testing

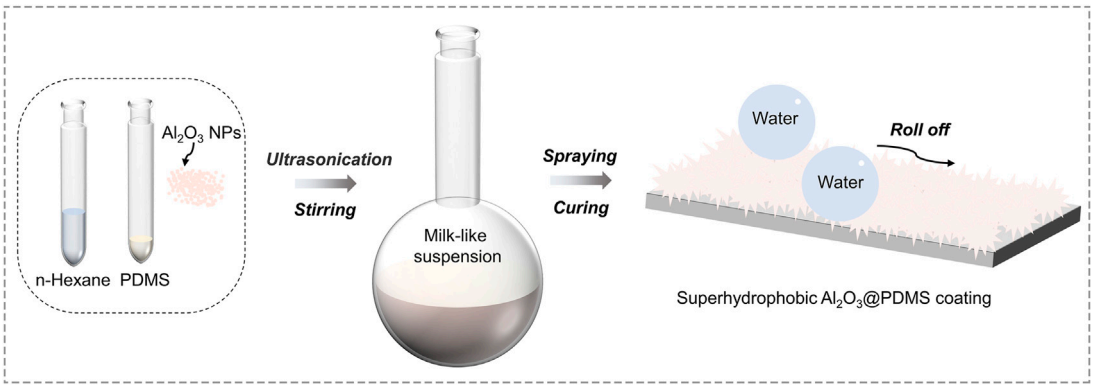


**FIGURE 1 |** Schematic illustration of the preparation procedure of the superhydrophobic $Al_2O_3$@PDMS composite coating.

frequency range of EIS is from 100 kHz to 10 mHz. The obtained EIS data were fitted with equivalent electrical circuit (EEC) using *Zsimwin* software. Potentiodynamic polarization curves were measured with respect to OCP in both the anodic and cathodic directions with a scanning speed of 0.167 mV/s. The corrosion current density ($I_{corr}$) and corrosion potential ($E_{corr}$) were calculated by extrapolating the linear portion of the curves with *CS Studio* software.

## Mechanical Robustness Test

The mechanical robustness of the fabricated superhydrophobic $Al_2O_3$@PDMS composite coating was assessed using the tape-peeling test and sandpaper abrasion tests. The prepared superhydrophobic coating was pressed with 3 M tape loaded with 100 g for 30 s to ensure a uniform contact between the 3 M tape and coating for the tape-peeling test. After that, the 3 M tape was completely peeled away from the surface. This press-peeling process was defined as one testing cycle. The abrasion test was carried out by orienting the as-fabricated superhydrophobic coating toward the 2,000-grit sandpaper and placing a weight of 100 g on top of it. The superhydrophobic coating was then subjected to unidirectional drift with a speed of 1 cm/s. One abrasion cycle was defined as the reciprocating pulling of the sample in the horizontal direction over a distance of 20 cm. After various tape-peeling and sandpaper abrasion cycles, the water contact angles and sliding angels of the samples were measured using a contact angle meter.

# RESULTS AND DISCUSSIONS

## Surface Wettability

The surface wettability of spray-coated $Al_2O_3$@PDMS composite coatings was investigated to understand and validate the optimal parameters. **Figure 2** depicts the variation of water contact angles and sliding angles of $Al_2O_3$@PDMS composite coatings with

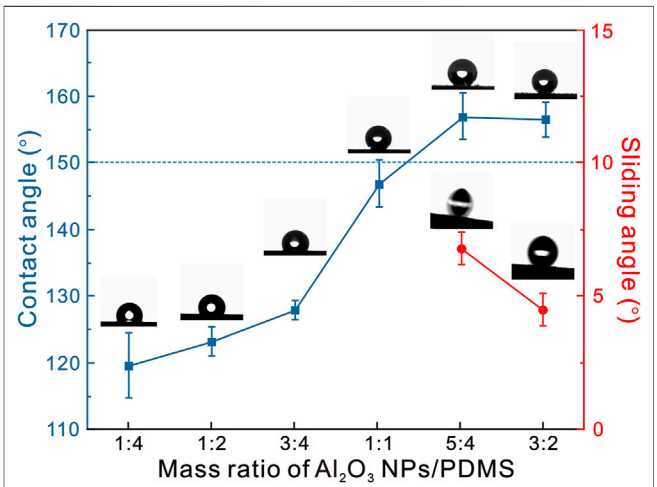


**FIGURE 2 |** Variation of water contact angles and sliding angles of the $Al_2O_3$@PDMS composite coatings with different $Al_2O_3$/PDMS mass ratios.

different $Al_2O_3$/PDMS mass ratios including 1:4, 1:2, 3:4, 1:1, 5:4, and 3:2. It can be seen that the water contact angles of the coatings gradually increased as the $Al_2O_3$/PDMS mass ratio increased. The contact angle of the $Al_2O_3$@PDMS composite coating was 119.6 ± 4.8°, 123.2 ± 2.2°, 127.9 ± 1.5°, and 146.9 ± 3.5°, corresponding to the $Al_2O_3$/PDMS mass ratios of 1:4, 1:2, 3:4, and 1:1, respectively. When the $Al_2O_3$/PDMS mass ratio is increased to 5:4, the water contact angle and sliding angle of the surface are 157.0 ± 3.5° and 6.7 ± 0.5°, respectively, displaying a typical superhydrophobic property. The water contact angle and the sliding angle are 156.5 ± 2.6° and 4.5 ± 0.5° when the $Al_2O_3$/PDMS mass ratio is 3:2. Surface superhydrophobicity was achieved through the combination of $Al_2O_3$ NP–induced roughness and low–surface energy PDMS molecules. The optimal $Al_2O_3$/PDMS mass ratio for developing superhydrophobic $Al_2O_3$@PDMS composite coating is 5:4, which was used to fabricate superhydrophobic samples for the characterizations and performance evaluations listed as follows.

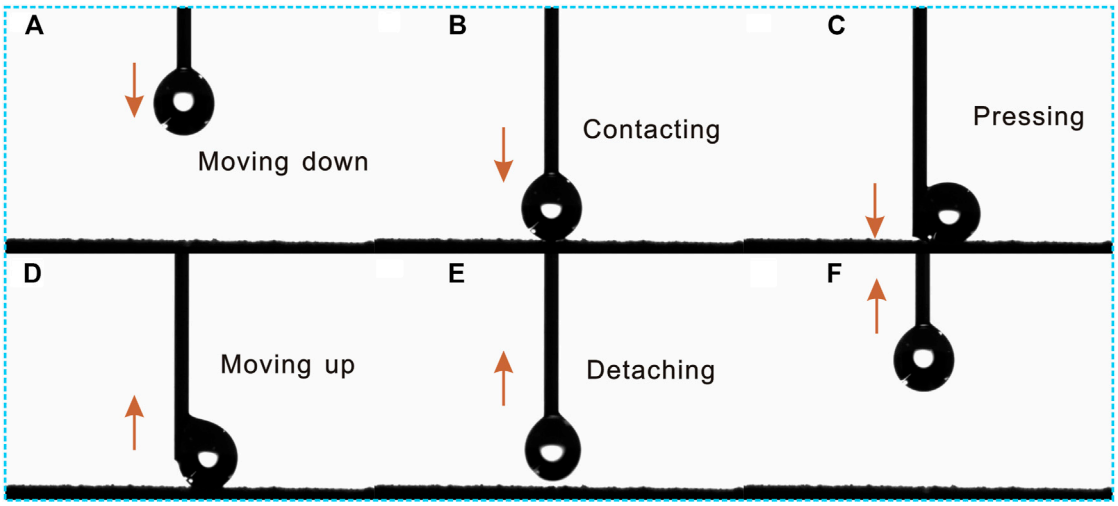


**FIGURE 3 | (A–F)** Dynamic contacting process of water droplet on the as-prepared superhydrophobic $Al_2O_3$@PDMS composite coating.

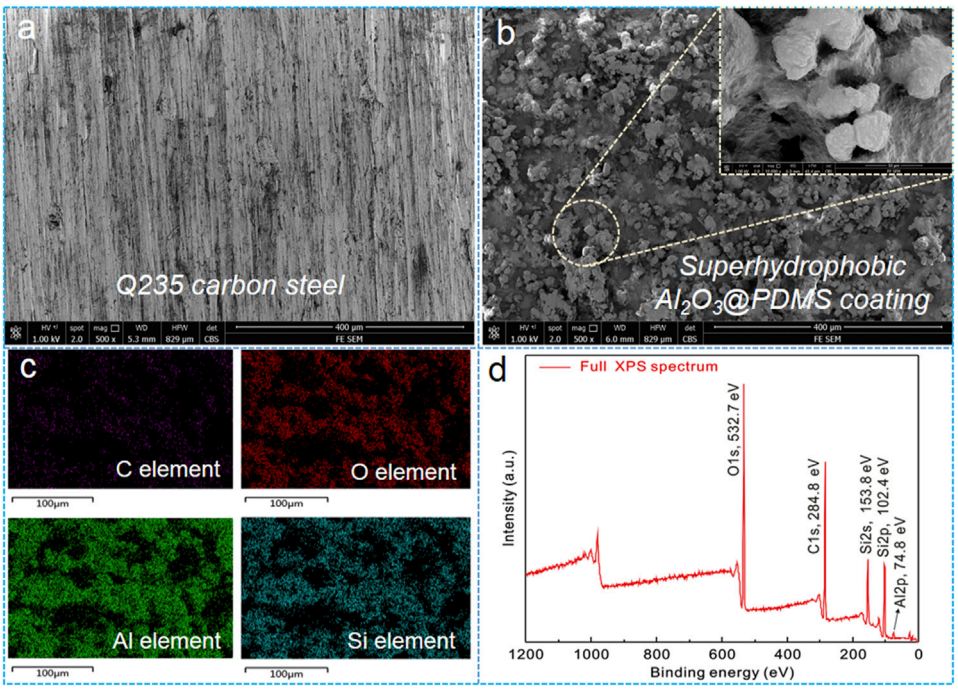


**FIGURE 4 | (A,B)** FE-SEM images of the bare Q235 carbon steel and the superhydrophobic $Al_2O_3$@PDMS coating, **(C)** EDS mappings, and **(D)** full XPS spectrum of the as-prepared superhydrophobic $Al_2O_3$@PDMS coating.

The dynamic contacting process of a water droplet on the as-prepared superhydrophobic $Al_2O_3$@PDMS composite coating is depicted in **Figure 3**. As the water droplet moves down from the microsyringe, it gradually closes and contacts with the as-prepared superhydrophobic Al2O3@PDMS composite coating (**Figures 3A,B**). As it is pressed further, the water droplet is pushed up and moved up along the neck of the microsyringe (**Figure 3C**). The water droplet detached and separated from the superhydrophobic $Al_2O_3$@PDMS coating as the microsyringe moved up, eventually hanging on the needlepoint of the microsyringe (**Figures 3D–F**). Throughout the dynamic process, the superhydrophobic surface remains non-wetting with no water traces remaining. As a result, the adhesion force between the superhydrophobic surface and the water droplet is

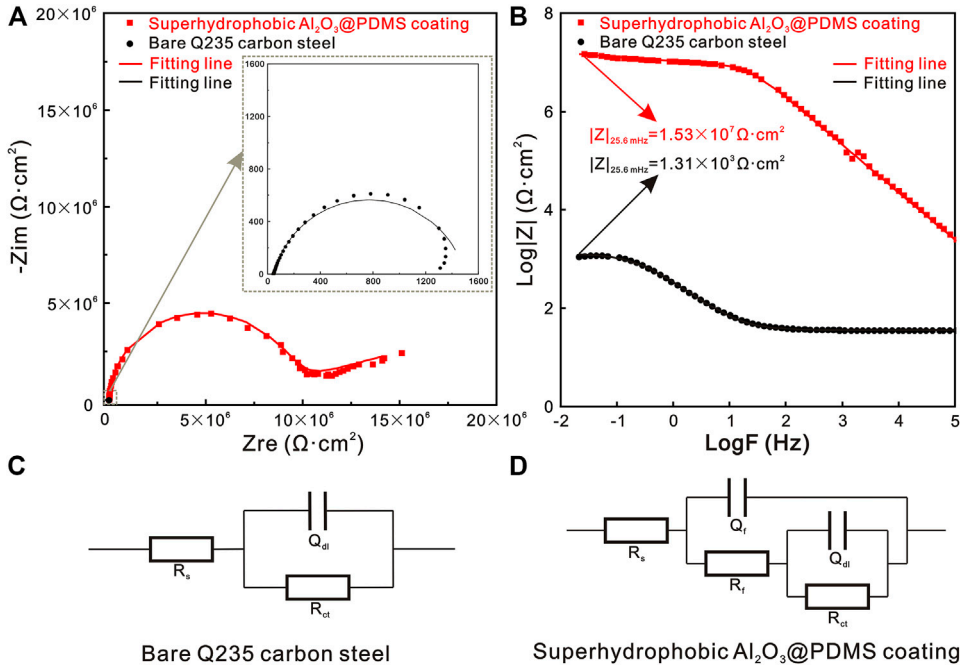


**FIGURE 5 | (A)** Nyquist plots, **(B)** Bode plots of log |Z| vs. log frequency, and **(C,D)** equivalent circuit models of the bare Q235 carbon steel and superhydrophobic $Al_2O_3$@PDMS coating.

extremely low, which contributes to the easy rolling behavior of liquids on the as-fabricated superhydrophobic $Al_2O_3$@PDMS coating.

## Surface Morphologies and Chemical Compositions

FE-SEM, EDS, and XPS techniques were used to observe the micro-/nano-structures and chemical compositions of the samples. **Figures 4A,B** present the SEM images of the bare Q235 carbon steel and superhydrophobic $Al_2O_3$@PDMS coating. The surface morphology of bare Q235 carbon steel is relatively smooth, with few sandpaper polishing marks, while for the superhydrophobic $Al_2O_3$@PDMS coating (shown in **Figure 4B**), some micro-sized clusters and protrusions with nano-sized particles (**Figure 4B** inset) were packed on the coating surface, resulting in a remarkably improved surface roughness. Theses micro- and nano-hierarchical structures can trap air to form an extremely thin layer of air cushion. The air cushion can significantly reduce the contacting area between the superhydrophobic $Al_2O_3$@PDMS coating and water droplets, which is crucial for the non-wetting Cassie–Baxter air–liquid–solid contact. As a result, the water droplets barely penetrate the as-fabricated superhydrophobic $Al_2O_3$@PDMS coating, demonstrating stable water-repellent superhydrophobicity.

Besides, the two-dimensional EDS mapping result of the fabricated superhydrophobic $Al_2O_3$@PDMS coating is presented in **Figure 4C**. According to the EDS mappings, the C, O, Al, and Si elements of the spray-coated superhydrophobic $Al_2O_3$@PDMS coating showed a uniform distribution. **Figure 4D** shows the full XPS spectrum of the as-prepared superhydrophobic $Al_2O_3$@PDMS coating. In this elemental analysis, five peak signals of Al2p, Si2p, Si2s, C1s, and O1s can be clearly observed in the XPS survey at the binding energies of 74.8, 102.4, 153.8, 284.8, and 532.7 eV, respectively. The results of the elemental testing indicate that the $Al_2O_3$ NPs@PDMS composite coating with superhydrophobicity was successfully produced.

## Anticorrosion Performance

The corrosion resistance behaviors of bare Q235 carbon steel and the as-prepared superhydrophobic $Al_2O_3$@PDMS coating in 3.5 wt.% NaCl aqueous solution were evaluated from the electrochemical points of view. Electrochemical impedance spectroscopy (EIS) is one of the most common techniques applied for the evaluation and analysis of the protective properties of coatings for metallic materials (Jeyaram et al., 2020; Mei et al., 2020). **Figure 5** presents the EIS plots and the equivalent circuit models of bare Q235 carbon steel and the superhydrophobic $Al_2O_3$@PDMS coating. **Figure 5A** and its inset image display the Nyquist plots of the Q235 carbon steel and superhydrophobic $Al_2O_3$@PDMS coating. The diameter of the capacitance arcs of the superhydrophobic $Al_2O_3$@PDMS coating is significantly larger than that of the bare Q235 carbon steel, demonstrating a superior anticorrosion properties. **Figure 5B** shows the Bode plots of log |Z| vs. log frequency of the Q235 carbon steel and superhydrophobic $Al_2O_3$@PDMS coating. The impedance modulus data at low frequency ($|Z|_{0.01\ Hz}$) are commonly used as an intuitive index of the anticorrosion

**TABLE 1 |** Electrochemical parameters for the EIS fitting results of bare Q235 carbon steel and superhydrophobic $Al_2O_3$@PDMS coating.

| Parameter | Bare Q235 carbon steel | Superhydrophobic $Al_2O_3$@PDMS coating |
|---|---|---|
| $R_s$ ($\Omega \cdot cm^2$) | 43.4 | 32.5 |
| $Q_f$ ($\Omega^{-1} \cdot cm^{-2} \cdot s^{n1}$) | — | $8.8 \times 10^{-10}$ |
| $n_1$ | — | 0.97 |
| $R_f$ ($\Omega \cdot cm^2$) | — | $8.4 \times 10^3$ |
| $Q_{dl}$ ($\Omega^{-1} \cdot cm^{-2} \cdot s^{n2}$) | $4.5 \times 10^{-4}$ | $2.3 \times 10^{-7}$ |
| $n_2$ | 0.84 | 0.79 |
| $R_{ct}$ ($\Omega \cdot cm^2$) | $1.5 \times 10^3$ | $3.3 \times 10^7$ |

barrier performance of protective coatings (Mishra et al., 2020; Wiering et al., 2021). According to the Bode plots of log |Z| vs. log frequency, the $|Z|_{0.01\ Hz}$ of the superhydrophobic $Al_2O_3$@PDMS coating is $1.53 \times 10^7\ \Omega \cdot cm^2$, which is four orders of magnitude higher than bare Q235 carbon steel ($1.31 \times 10^3\ \Omega \cdot cm^2$), indicating that the superhydrophobic $Al_2O_3$@PDMS coating can lead to excellent corrosion protection properties.

To perform a quantitative comparison, the EIS data were fitted using equivalent circuit models. **Figures 5C,D** show the equivalent circuit model of the bare Q235 carbon steel and the superhydrophobic $Al_2O_3$@PDMS coating. The $R_s(Q_{dl}R_{ct})$ equivalent circuit model was used for the EIS fitting of bare Q235 carbon steel. $R_s$, $Q_{dl}$, and $R_{ct}$ refer to solution resistance, constant phase element of the electric double layer, and charge transfer resistance at Q235 carbon steel/electrolyte interface, respectively. As a comparison, the $R_s\{Q_f[R_f(Q_{dl}R_{ct})]\}$ equivalent circuit model was employed for the as-prepared superhydrophobic $Al_2O_3$@PDMS coating, in which $Q_f$ and $R_f$ represent the constant phase element and film resistance of superhydrophobic $Al_2O_3$@PDMS coating, respectively. The corresponding fitting parameters are provided in **Table 1**. The lower $Q_{dl}$ and higher $R_{ct}$ values of the superhydrophobic $Al_2O_3$@PDMS coating suggest a conspicuously reduced corrosion rate.

Generally, a lower corrosion current density ($I_{corr}$) or a higher corrosion potential ($E_{corr}$) in a typical potentiodynamic polarization curve corresponds to a lower corrosion rate and higher corrosion resistance (Mishra and Balasubramaniam, 2004; Liu et al., 2016). **Figure 6** shows the potentiodynamic polarization curves of bare Q235 carbon steel and the as-prepared superhydrophobic $Al_2O_3$@PDMS coating in 3.5 wt.% NaCl aqueous solution. The corrosion potential ($E_{corr}$) and corrosion current density ($I_{corr}$) of the as-prepared superhydrophobic $Al_2O_3$@PDMS coating are −0.52 V and $3.74 \times 10^{-10}$ A/cm$^2$, respectively, indicating a remarkable difference from that of the bare Q235 carbon steel ($E_{corr}$ = −0.80 V, $I_{corr} = 4.66 \times 10^{-6}$ A/cm$^2$). The $E_{corr}$ of the as-fabricated superhydrophobic $Al_2O_3$@PDMS coating shifted toward the positive direction by 0.27 V and the $I_{corr}$ decreased by more than four orders of magnitude. The significant positive shift of the $E_{corr}$ could be attributed to the improved protective performance of the as-fabricated superhydrophobic $Al_2O_3$@PDMS coating. The corresponding corrosion inhibition efficiency ($\eta$) could be calculated using the equation as follows (Liu et al., 2020; Ma et al., 2020):

$$\eta = \frac{I_{corr}^{bare} - I_{corr}^{coating}}{I_{corr}^{bare}} \times 100\%. \quad (1)$$

According to **Eq. 1**, the $\eta$ value of the as-fabricated superhydrophobic $Al_2O_3$@PDMS coating was calculated to be 99.992%, supporting the conclusion that the spray-coated superhydrophobic $Al_2O_3$@PDMS coating provides an effective barrier for corrosion suppression.

## Deliquescence Behaviors of NaCl Salt Particles

Atmospheric corrosion of metallic materials is a spontaneous degradation process resulting from interactions with its surrounding environment (Pei et al., 2020). More frequently, the atmospheric corrosion processes are initiated by surface wetting due to the moisture condensation and hygroscopic properties of salts and pollutants deposited on the surface (Koushik et al., 2021). Thus, understanding the interaction and relationship between NaCl salt particles and the atmospheric environment with high relative humidity remains a major challenge. To address this issue, the hygroscopic and deliquesce behaviors of single and double NaCl salt particles were investigated, as shown in **Figure 7**.

**Figures 7A–D** depict the deliquescence process of a single NaCl particle on a horizontally placed superhydrophobic $Al_2O_3$@PDMS coating in an atmospheric condition with 80 ± 2% relative humidity. Water vapor condensed on the surface of the solid NaCl particle during the deliquesce process, forming a saline solution. The solid NaCl particle was completely dissolved after deliquesce for 95 min, presenting a spherical saline liquid droplet. Owing to the liquid-repellent superhydrophobicity, the saline solution could not spread and wet the coating, resulting in a good protective performance against NaCl salt deliquesce–induced atmospheric corrosion attack. In addition, the deliquesce

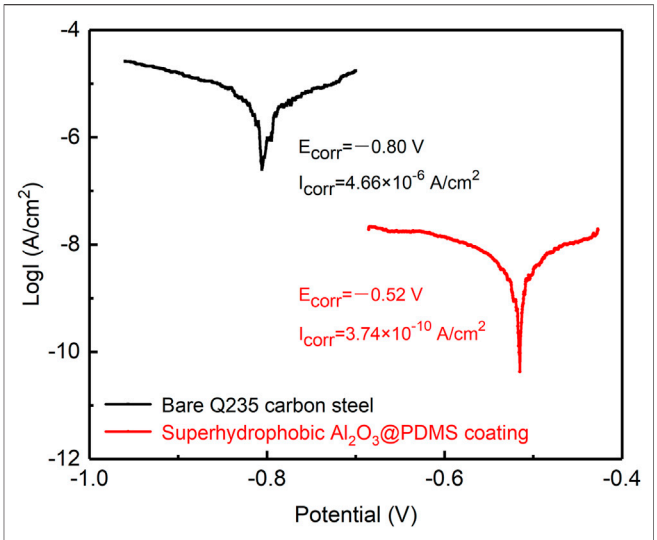


**FIGURE 6 |** Potentiodynamic polarization curves of the bare Q235 carbon steel and the as-prepared superhydrophobic $Al_2O_3$@PDMS coating with a scanning rate of 0.167 mV/s.

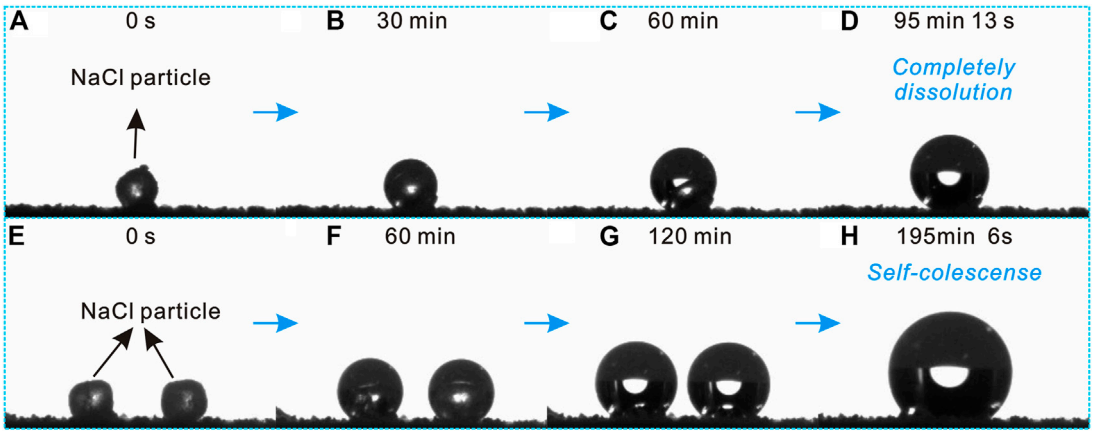


**FIGURE 7 |** Deliquescence behaviors of **(A–D)** single and **(E–H)** double NaCl salt particles on the prepared superhydrophobic $Al_2O_3$@PDMS coating under relative humidity environment of 80 ± 2%.

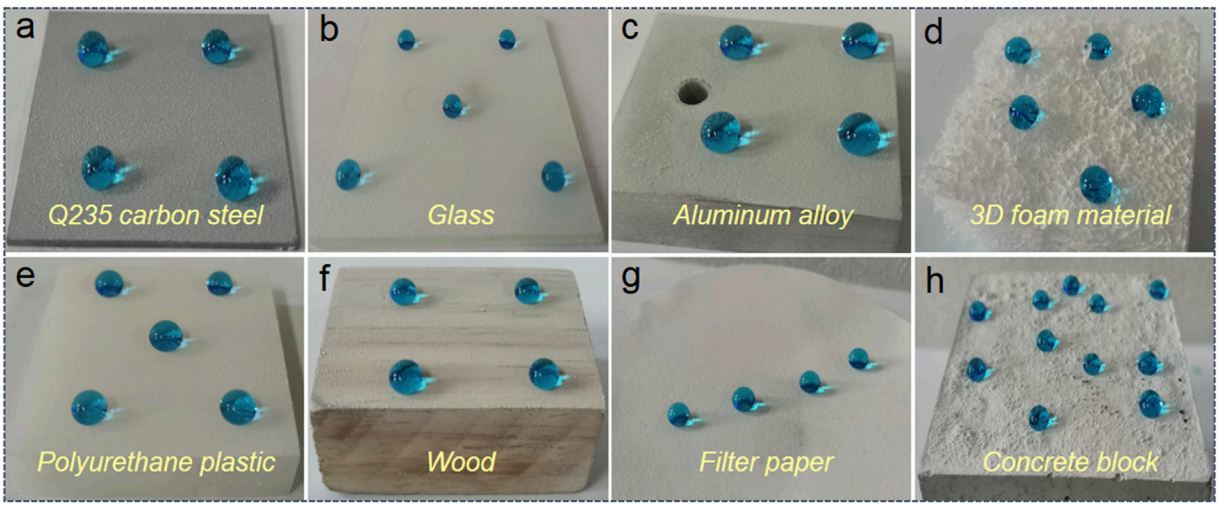


**FIGURE 8 |** Optical images of superhydrophobic $Al_2O_3$@PDMS coating on different substrates including **(A)** Q235 carbon steel, **(B)** glass, **(C)** aluminum alloy, **(D)** 3D foam material, **(E)** polyurethane plastic, **(F)** wood, **(G)** filter paper, and **(H)** concrete block.

behavior of double NaCl salt particles on the prepared superhydrophobic $Al_2O_3$@PDMS coating was first carried out and studied, as depicted in **Figures 7E–H**. At the beginning of the deliquescence process, the evolution of the double NaCl particles was similar to that of the single NaCl salt deliquesce. The solution film formed over the double NaCl particles, resulting in larger spherical droplets as deliquescence time passed. With the deliquescence time prolonged to 195 min 6 s (**Figure 7H**), it is worth noting that the two saline solution droplets self-coalesced instantaneously and eventually became a single saline droplet. The self-coalescence–induced salt deliquescence behavior of the as-fabricated superhydrophobic $Al_2O_3$@PDMS coating demonstrates that the Cassie–Baxter interfacial phase contacts of the superhydrophobic surface can serve as an efficient barrier to suppress the formation of thin saline liquid electrolyte film and protect the underlying substrate from being corroded under the atmospheric service environments with high relative humidity.

## Adaptability and Mechanical Robustness

The adaptability of superhydrophobic coatings is critical for real-world applications. The preparation procedure should be adaptable to various substrates. To demonstrate the substrate-independent property of the as-fabricated superhydrophobic $Al_2O_3$@PDMS coating, eight typical substrates were used to study the large-scale adaptability performance, including Q235 carbon steel, glass, aluminum alloy, 3D foam material, polyurethane plastic, wood, filter paper, and concrete block. **Figures 8A–H** show the optical images of the spray-coated superhydrophobic $Al_2O_3$@PDMS coating on different substrates. The dyed blue water droplets maintained a spherical shape on each spray-coated substrate, illustrating a typical Cassie–Baxter

**TABLE 2 |** Water contact angles and sliding angles of the obtained superhydrophobic coating on different substrates.

| Substrate | Contact angles | Sliding angles |
|---|---|---|
| Q235 carbon steel | 157.0 ± 3.5° | 6.7 ± 0.5° |
| Glass | 156.2 ± 3.0° | 5.4 ± 0.5° |
| Aluminum alloy | 155.6 ± 2.5° | 5.7 ± 1.0° |
| 3D foam material | 157.8 ± 2.0° | 7.0 ± 0.5° |
| Polyurethane plastic | 156.5 ± 3.0° | 6.0 ± 1.0° |
| Wood | 158.3 ± 2.5° | 4.5 ± 1.5° |
| Filter paper | 158.0 ± 3.0° | 5.0 ± 2.0° |
| Concrete block | 159.1 ± 3.5° | 6.5 ± 1.0° |

interfacial phase contact. The water contact angles and sliding angles of the obtained superhydrophobic coating on different substrates are presented in **Table 2**. The contact angles were all greater than 150° with sliding angles less than 8°, indicating excellent superhydrophobicity. It is noteworthy that the facile and substrate-independent spray coating method and the fluorine-free superhydrophobic $Al_2O_3$@PDMS coating will provide a suitable large-scale technique that can be easily applied to various substrates and has potential applications for water repellency, self-cleaning, corrosion resistance, and so on.

Mechanical robustness plays a key role for functional applications. Tape peeling and sandpaper abrasion tests are commonly conducted to evaluate the mechanical robustness and durability of superhydrophobic materials. **Figures 9A,B** present the variations of water contact angles and sliding angles of the superhydrophobic $Al_2O_3$@PDMS coating after different cycles in the tape peeling and sandpaper abrasion tests. After 32 tape peeling cycles, the as-prepared superhydrophobic $Al_2O_3$@PDMS coating remained its superhydrophobic property with a contact angle of 152.4 ± 2.2° and a sliding angle of 9.8 ± 0.6°. The sandpaper abrasion test was performed to confirm the mechanical durability. As shown in **Figure 9B**, the contact angles of the superhydrophobic $Al_2O_3$@PDMS coating decrease by only 5° after 20 abrasion cycles (i.e., 400 cm length) with a contact angle of 153.6 ± 1.8°. The results of the tape peeling and sandpaper abrasion tests show that the fabricated superhydrophobic $Al_2O_3$@PDMS coating possesses excellent mechanical robustness and durability. The cross-linked PDMS can firmly bind the $Al_2O_3$ NPs and contribute to the improvement of the mechanical strength of the coating.

## CONCLUSION

In summary, eco-friendly and robust superhydrophobic $Al_2O_3$@PDMS coating was fabricated through a facile one-step substrate-independent spray coating approach without the use of hazardous fluorochemicals. The $Al_2O_3$ NP–induced micro-/nano-roughness and PDMS with low surface energy both contribute to the achievement of water-repellent superhydrophobicity. The optimal $Al_2O_3$/PDMS mass ratio for developing superhydrophobic $Al_2O_3$@PDMS composite coating is 5:4. The as-prepared superhydrophobic coating exhibits extremely low adhesion force between the water droplet and the solid surface. The $|Z|_{0.01\ Hz}$ value of Bode plots of the superhydrophobic $Al_2O_3$@PDMS coating is $1.53 \times 10^7\ \Omega{\cdot}cm^2$, which is four orders of magnitude higher than that of the bare Q235 carbon steel ($1.31 \times 10^3\ \Omega{\cdot}cm^2$), indicating excellent corrosion protection properties. Furthermore, the $E_{corr}$ of the superhydrophobic $Al_2O_3$@PDMS coating shifted toward the positive direction by 0.27 V and the $I_{corr}$ reduced by more than four orders of magnitude. The deliquescence behaviors of the single and double NaCl salt particles on the as-fabricated superhydrophobic $Al_2O_3$@PDMS coating present spherical saline droplets and instantaneous self-coalescence phenomenon, indicating that the Cassie–Baxter interfacial phase contacts of the superhydrophobic surface can serve as an efficient barrier to suppress the atmospheric corrosion in high relative humidity marine and industrial environments.

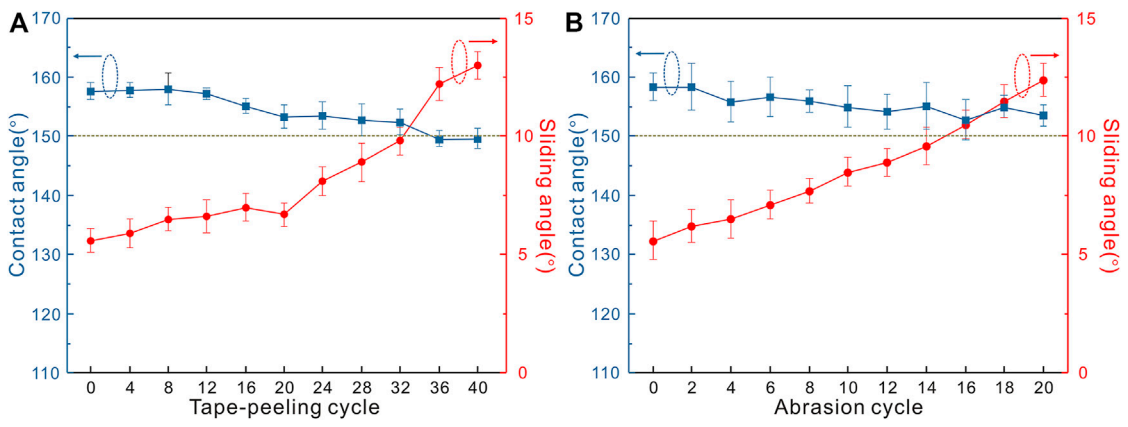


**FIGURE 9 |** Variations of water contact angles and sliding angles of the superhydrophobic $Al_2O_3$@PDMS coating after different **(A)** tape peeling and **(B)** sandpaper abrasion cycles.

## DATA AVAILABILITY STATEMENT

The original contributions presented in the study are included in the article/Supplementary Material; further inquiries can be directed to the corresponding author.

## AUTHOR CONTRIBUTIONS

BZ contributed to conceptualization, methodology, writing-original draft, funding acquisition, and supervision; JY contributed to data curation, formal analysis, and software; WX contributed to software; TY contributed to data curation; ZC contributed to writing—review and editing; and JD contributed to writing—review and editing. All authors have read and approved the submitted article version for publication.

## ACKNOWLEDGMENTS

The authors acknowledge the financial supports from the Project of Innovation Development Joint Funds supported by the Shandong Provincial Natural Science Foundation (No. ZR2021LFG004); the Youth Innovation Promotion Association Chinese Academy of Sciences (No. 2021207); and the 2020 Open Projects (No. KLATM202006) of Key Laboratory of Advanced Technologies of Materials, Ministry of Education China, Southwest Jiaotong University.

## REFERENCES

Anitha, C., Syed Azim, S., and Mayavan, S. (2018). Influence of Particle Size in Fluorine Free Corrosion Resistance Superhydrophobic Coating - Optimization and Stabilization of Interface by Multiscale Roughness. *J. Alloys Compd.* 765, 677–684. doi:10.1016/j.jallcom.2018.06.214

Boinovich, L. B., Emelyanenko, K. A., Domantovsky, A. G., and Emelyanenko, A. M. (2018). Laser Tailoring the Surface Chemistry and Morphology for Wear, Scale and Corrosion Resistant Superhydrophobic Coatings. *Langmuir* 34, 7059–7066. doi:10.1021/acs.langmuir.8b01317

Darband, G. B., Aliofkhazraei, M., Khorsand, S., Sokhanvar, S., and Kaboli, A. (2020). Science and Engineering of Superhydrophobic Surfaces: Review of Corrosion Resistance, Chemical and Mechanical Stability. *Arabian J. Chem.* 13, 1763–1802. doi:10.1016/j.arabjc.2018.01.013

Du, X. Q., and Chen, Y. (2020). Corrosion Inhibition by a Superhydrophobic Surface on Aluminum that Was Prepared with a Facile Electrochemical Route. *Mater. Res. Express* 7, 056405. doi:10.1088/2053-1591/ab9253

Esmaeili, A. R., Mir, N., and Mohammadi, R. (2020). A Facile, Fast, and Low-Cost Method for Fabrication of Micro/nano-Textured Superhydrophobic Surfaces. *J. Colloid Interf. Sci.* 573, 317–327. doi:10.1016/j.jcis.2020.04.027

Jena, G., Thinaharan, C., George, R. P., and Philip, J. (2020). Robust Nickel-Reduced Graphene Oxide-Myristic Acid Superhydrophobic Coating on Carbon Steel Using Electrochemical Codeposition and its Corrosion Resistance. *Surf. Coat. Techn.* 397, 125942. doi:10.1016/j.surfcoat.2020.125942

Jeyaram, R., Elango, A., Siva, T., Ayeshamariam, A., and Kaviyarasu, K. (2020). Corrosion protection of Silane Based Coatings on Mild Steel in an Aggressive Chloride Ion Environment. *Surf. Inter.* 18, 100423. doi:10.1016/j.surfin.2019.100423

Koushik, B. G., Van den Steen, N., Mamme, M. H., Van Ingelgem, Y., and Terryn, H. (2021). Review on Modelling of Corrosion under Droplet Electrolyte for Predicting Atmospheric Corrosion Rate. *J. Mater. Sci. Techn.* 62, 254–267. doi:10.1016/j.jmst.2020.04.061

Lan, X., Zhang, B., Wang, J., Fan, X., and Zhang, J. (2021). Hydrothermally Structured Superhydrophobic Surface with superior Anti-corrosion, Anti-bacterial and Anti-icing Behaviors. *Colloids Surf. A Physicochem. Eng. Aspects* 624, 126820. doi:10.1016/j.colsurfa.2021.126820

Liu, W., Xu, Q., Han, J., Chen, X., and Min, Y. (2016). A Novel Combination Approach for the Preparation of Superhydrophobic Surface on Copper and the Consequent Corrosion Resistance. *Corrosion Sci.* 110, 105–113. doi:10.1016/j.corsci.2016.04.015

Liu, X., Zhang, T. C., He, H., Ouyang, L., and Yuan, S. (2020). A Stearic Acid/CeO2 Bilayer Coating on AZ31B Magnesium alloy with Superhydrophobic and Self-Cleaning Properties for Corrosion Inhibition. *J. Alloys Compd.* 834, 155210. doi:10.1016/j.jallcom.2020.155210

Ma, Y., Fan, B., Liu, H., Fan, G., Hao, H., and Yang, B. (2020). Enhanced Corrosion Inhibition of Aniline Derivatives Electropolymerized Coatings on Copper: Preparation, Characterization and Mechanism Modeling. *Appl. Surf. Sci.* 514, 146086. doi:10.1016/j.apsusc.2020.146086

Mei, D., Lamaka, S. V., Lu, X., and Zheludkevich, M. L. (2020). Selecting Medium for Corrosion Testing of Bioabsorbable Magnesium and Other Metals - A Critical Review. *Corrosion Sci.* 171, 108722. doi:10.1016/j.corsci.2020.108722

Mishra, R., and Balasubramaniam, R. (2004). Effect of Nanocrystalline Grain Size on the Electrochemical and Corrosion Behavior of Nickel. *Corrosion Sci.* 46, 3019–3029. doi:10.1016/j.corsci.2004.04.007

Mishra, P., Yavas, D., Bastawros, A. F., and Hebert, K. R. (2020). Electrochemical Impedance Spectroscopy Analysis of Corrosion Product Layer Formation on Pipeline Steel. *Electrochim. Acta* 346, 136232. doi:10.1016/j.electacta.2020.136232

Mokhtari, S., Karimzadeh, F., Abbasi, M. H., and Raeissi, K. (2017). Development of Super-hydrophobic Surface on Al 6061 by Anodizing and the Evaluation of its Corrosion Behavior. *Surf. Coat. Techn.* 324, 99–105. doi:10.1016/j.surfcoat.2017.05.060

Oguzie, E. E., Enenebeaku, C. K., Akalezi, C. O., Okoro, S. C., Ayuk, A. A., and Ejike, E. N. (2010). Adsorption and Corrosion-Inhibiting Effect of *Dacryodis Edulis* Extract on Low-Carbon-Steel Corrosion in Acidic media. *J. Colloid Interf. Sci.* 349, 283–292. doi:10.1016/j.jcis.2010.05.027

Panda, J. N., Wong, B. C., Medvedovski, E., and Egberts, P. (2021). Enhancement of Tribo-Corrosion Performance of Carbon Steel through Boronizing and BN-Based Coatings. *Tribology Int.* 153, 106666. doi:10.1016/j.triboint.2020.106666

Pei, Z., Zhang, D., Zhi, Y., Yang, T., Jin, L., Fu, D., et al. (2020). Towards Understanding and Prediction of Atmospheric Corrosion of an Fe/Cu Corrosion Sensor via Machine Learning. *Corrosion Sci.* 170, 108697. doi:10.1016/j.corsci.2020.108697

Sataeva, N. E., Boinovich, L. B., Emelyanenko, K. A., Domantovsky, A. G., and Emelyanenko, A. M. (2020). Laser-assisted Processing of Aluminum alloy for the Fabrication of Superhydrophobic Coatings Withstanding Multiple Degradation Factors. *Surf. Coat. Techn.* 397, 125993. doi:10.1016/j.surfcoat.2020.125993

Tan, J., Guo, L., Yang, H., Zhang, F., and El Bakri, Y. (2020). Synergistic Effect of Potassium Iodide and Sodium Dodecyl Sulfonate on the Corrosion Inhibition of Carbon Steel in HCl Medium: a Combined Experimental and Theoretical Investigation. *RSC Adv.* 10, 15163–15170. doi:10.1039/D0RA02011G

Wang, F., and Guo, Z. (2018). Insitu Growth of Durable Superhydrophobic Mg-Al Layered Double Hydroxides Nanoplatelets on Aluminum Alloys for Corrosion Resistance. *J. Alloys Compd.* 767, 382–391. doi:10.1016/j.jallcom.2018.07.086

Wang, C.-X., and Zhang, X.-F. (2020). A Non-particle and Fluorine-free Superhydrophobic Surface Based on One-step Electrodeposition of Dodecyltrimethoxysilane on Mild Steel for Corrosion protection. *Corrosion Sci.* 163, 108284. doi:10.1016/j.corsci.2019.108284

Wiering, L., Qi, X., and Battocchi, D. (2021). Corrosion Performance of High-Temperature Organic Coatings Subjected to Heat Treatments. *Prog. Org. Coat.* 159, 106418. doi:10.1016/j.porgcoat.2021.106418

Ye, Y., Chen, H., Zou, Y., Ye, Y., and Zhao, H. (2020). Corrosion Protective Mechanism of Smart Graphene-Based Self-Healing Coating on Carbon Steel. *Corrosion Sci.* 174, 108825. doi:10.1016/j.corsci.2020.108825

Zhang, B., Xu, W., Zhu, Q., Sun, Y., and Li, Y. (2019a). Mechanically Robust Superhydrophobic Porous Anodized AA5083 for marine Corrosion protection. *Corrosion Sci.* 158, 108083. doi:10.1016/j.corsci.2019.06.031

Zhang, B., Xu, W., Zhu, Q., Yuan, S., and Li, Y. (2019b). Lotus-inspired Multiscale Superhydrophobic AA5083 Resisting Surface Contamination and marine Corrosion Attack. *Materials* 12, 1592. doi:10.3390/ma12101592

Zhang B, B., Wang, J., and Zhang, J. (2020). One-pot Fluorine-free Superhydrophobic Surface towards Corrosion Resistance and Water Droplet Bouncing. *Mater. Corrosion* 71, 2011–2020. doi:10.1002/maco.202011787

Zhang S, S., Hou, L., Du, H., Wei, H., Liu, B., and Wei, Y. (2020). A Study on the Interaction between Chloride Ions and CO2 towards Carbon Steel Corrosion. *Corrosion Sci.* 167, 108531. doi:10.1016/j.corsci.2020.108531

Zhang ZQ, Z.-Q., Zeng, R.-C., Yan, W., Lin, C.-G., Wang, L., Wang, Z.-L., et al. (2020). Corrosion Resistance of One-step Superhydrophobic Polypropylene Coating on Magnesium Hydroxide-Pretreated Magnesium alloy AZ31. *J. Alloys Compd.* 821, 153515. doi:10.1016/j.jallcom.2019.153515

Zhang, B., and Xu, W. (2021). Superhydrophobic, Superamphiphobic and SLIPS Materials as Anti-corrosion and Anti-biofouling Barriers. *New J. Chem.* 45, 15170–15179. doi:10.1039/D1NJ03158A

Zhang B, B., Duan, J., Huang, Y., and Hou, B. (2021). Double Layered Superhydrophobic PDMS-Candle Soot Coating with Durable Corrosion Resistance and thermal-mechanical Robustness. *J. Mater. Sci. Techn.* 71, 1–11. doi:10.1016/j.jmst.2020.09.011

Zhang ZQ, Z.-Q., Wang, L., Zeng, M.-Q., Zeng, R.-C., Lin, C.-G., Wang, Z.-L., et al. (2021). Corrosion Resistance and Superhydrophobicity of One-step Polypropylene Coating on Anodized AZ31 Mg alloy. *J. Magnesium Alloys* 9, 1443–1457. doi:10.1016/j.jma.2020.06.011

**Conflict of Interest:** The authors declare that the research was conducted in the absence of any commercial or financial relationships that could be construed as a potential conflict of interest.

**Publisher's Note:** All claims expressed in this article are solely those of the authors and do not necessarily represent those of their affiliated organizations, or those of the publisher, the editors, and the reviewers. Any product that may be evaluated in this article, or claim that may be made by its manufacturer, is not guaranteed or endorsed by the publisher.